SIViP (2017) 11:945–952
DOI 10.1007/s11760-016-1043-x

ORIGINAL PAPER

Optic disc and cup segmentation by automatic thresholding with morphological operation for glaucoma evaluation

Anindita Septiarini[1,3] · **Agus Harjoko**[1] · **Reza Pulungan**[1] · **Retno Ekantini**[2]

Received: 16 June 2016 / Revised: 26 November 2016 / Accepted: 7 December 2016 / Published online: 20 December 2016

Abstract This research proposes a robust method for disc localization and cup segmentation that incorporates masking to avoid misclassifying areas as well as forming the structure of the cup based on edge detection. Our method has been evaluated using two fundus image datasets, namely: D-I and D-II comprising of 60 and 38 images, respectively. The proposed method of disc localization achieves an average F_{score} of 0.96 and average boundary distance of 7.7 for D-I, and 0.96 and 9.1, respectively, for D-II. The cup segmentation method attains an average F_{score} of 0.88 and average boundary distance of 13.8 for D-I, and 0.85 and 18.0, respectively, for D-II. The estimation errors (mean $\pm$ standard deviation) of our method for the value of vertical cup-to-disc diameter ratio against the result of the boundary by the expert of D-I and D-II have similar value, namely 0.04 ± 0.04. Overall, the result of our method indicates its robustness for glaucoma evaluation.

✉ Anindita Septiarini
anindita.septiarini@gmail.com

Agus Harjoko
aharjoko@ugm.ac.id

Reza Pulungan
pulungan@ugm.ac.id

Retno Ekantini
rekantini@ugm.ac.id

[1] Department of Computer Science and Electronics, Faculty of Mathematics and Natural Sciences, Universitas Gadjah Mada, Yogyakarta 55281, Indonesia

[2] Faculty of Medicine, Universitas Gadjah Mada, Yogyakarta 55281, Indonesia

[3] Department of Computer Science, Mulawarman University, Samarinda 75123, Indonesia

Keywords Glaucoma · Disc segmentation · Cup segmentation · Thresholding · Morphology

1 Introduction

Glaucoma is the world's second biggest cause of blindness [1]. The disease cannot be cured and causes a decreasing function of vision and may cause blindness. The main characteristics of glaucoma is the changing of the structure of the optic nerve head (ONH) [2]. ONH or disc is an area with a round form, in the inside of which resides a smaller round area called cup. The part located between the boundary of the disc and the cup is called the neuroretinal rim. There are many types of images to observe the structure of the disc such as retinal fundus, optical coherence tomography (OCT) and Heidelberg retina tomograph (HRT) [2]. This research uses fundus images as experimental data because fundus cameras are available almost in all primary health-care providers and they can be used to observe other diseases in retina, such as hypertensive retinopathy and diabetic retinopathy. An example of a fundus image and the structure of its ONH are shown in Fig. 1.

There are several characteristics that can be used to determine the occurrence of glaucoma in a patient: vertical cup-to-disc diameter ratio (CDR) value, the compatibility of inferior, superior, nasal and temporal (ISNT) rules (in normal eyes, I has the highest value followed by S, N, and T), the presence of haemorrhage, and parapapillary atrophy (PPA) beta-zone. In this research, the occurrence of glaucoma is evaluated by using CDR and ISNT characteristics only.

Glaucoma evaluation is required to implement the detection of glaucoma, since early symptoms of this disease are usually not felt by the patient and the development of the disease can be slow. Because of these, when the disease

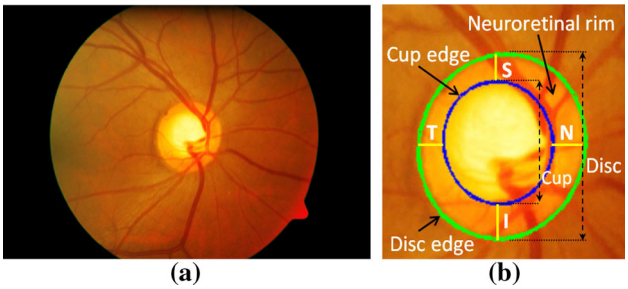

Fig. 1 **a** An example of a fundus image, **b** the structure of ONH

is finally detected, the damage occurring on disc may have already been severe. Glaucoma is an incurable disease, but if it is detected early, medication and procedure are available to decelerate the progress of the disease.

Researches on computer-assisted glaucoma detection techniques have flourished over the last 5 years. Most of these techniques involve automatic measurement of CDR from input images. To accomplish this, segmentation of the disc and cup must be applied.

Several methods have been proposed for disc and cup segmentation using fundus image. Automated segmentation methods for disc and cup include thresholding [3,4], active contour [5–9], superpixel [10–12], region growing [13,14] and clustering [7,15,16]. In order to more easily distinguish disc and cup areas from other objects, several researches used specific colour space. Disc area is more easily segmented in colour space of red [4,14,17–19], green [18,20–22], blue [3,21,23], HSI [24] and HSV [25]. For cup area, it is more suitable to use green colour [6,15,17,26]. In order to obtain better cup area, additional information based on the structure of vessels' bends was used, as a reference to mark cup boundary [8]. Cup segmentation is more challenging than disc segmentation, since blood vessels are present in the cup area. Therefore, blood vessels removal (BVR) [3,9,11,13,17] is needed.

Currently, glaucoma detection researches that make use of the characteristics of ISNT are still limited. Those researches have different ways of determining the ISNT values: based on the number of blood vessels [17] in each sector of I, S, N and T, based on the area of neuroretinal rim [25] in a particular quadrant, or based on the distance between cup and disc [6,13]. In this research, we propose a glaucoma evaluation method that obtains the values of CDR and ISNT automatically within the disc–cup segmentation process. We will show that our proposed method is robust for the datasets we experiment on. The main contributions of this research are:

- A new disc localization method that makes use of the border mask to avoid misclassifying areas,
- A new cup segmentation method that forms the structure of cup using edge detection and cup mask,
- A new eye detection method to determine whether a fundus image contains the right or the left eye using a simple thresholding.

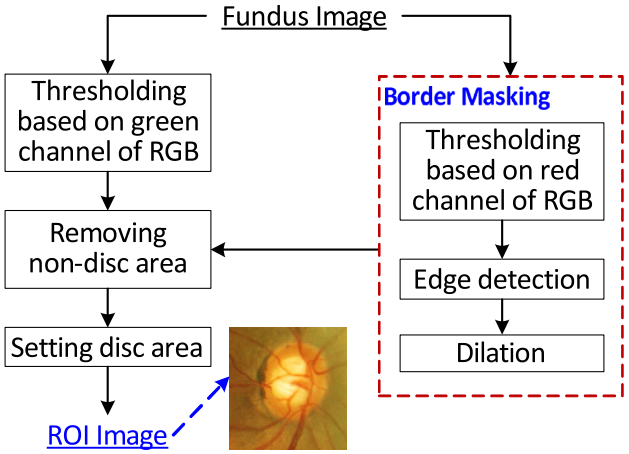

Fig. 2 The overview of the disc localization process

This paper is organized as follows. We describe the proposed method in Sect. 2. Two different datasets and the experimental setup are presented in Sect. 3. Section 4 presents our experimental results. Finally, Sect. 5 concludes the paper.

2 Proposed method

2.1 Disc localization

The values of all parameters–namely, for thresholding, median filtering, and morphological operations–used in our method are selected by empirically experimenting with several possible different values and choosing the best.

This process is applied as has been done in several previous researches [24,27,28]. This process aims at forming a sub-image that contains the whole disc, namely region of interest (ROI) image, to simplify subsequent process. The steps of our disc localization method are depicted in Fig. 2. Disc in fundus images is usually of high intensity value that can be seen more clearly in the green channel. Subsequently, thresholding is aimed at predicting the location of the disc centre as has been done in a previous research [29]. In this research, it is applied based on green colour channel with the value of threshold 1/5 of the highest intensity value. This thresholding, however, may produce misclassified area around the edge of retina, which is caused by inappropriate image acquisition. To overcome this, we propose to perform border masking. Firstly, we apply Otsu's thresholding by the red colour channel of the fundus images followed by Sobel edge detection. The final result is used as a reference to form border mask by applying dilation using strel size 90. Lastly,

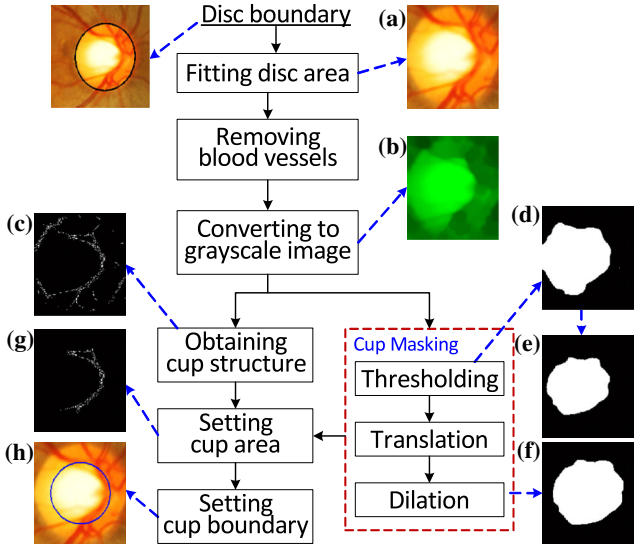

Fig. 3 The overview of cup segmentation process and the resulting image of each step: **a** ROI cup, **b** non-blood vessel, **c** cup structure, **d** initial threshold, **e** final threshold, **f** cup mask, **g** reference cup boundary, **h** cup boundary

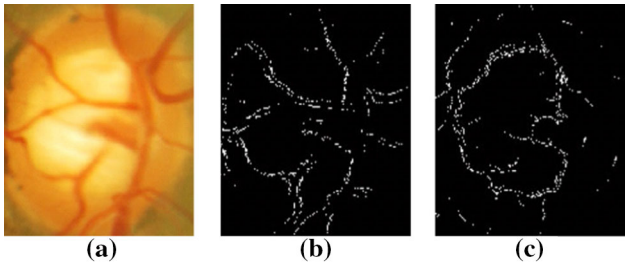

Fig. 4 The result of cup structuring process: **a** original image, **b** without BVR process, **c** with BVR process

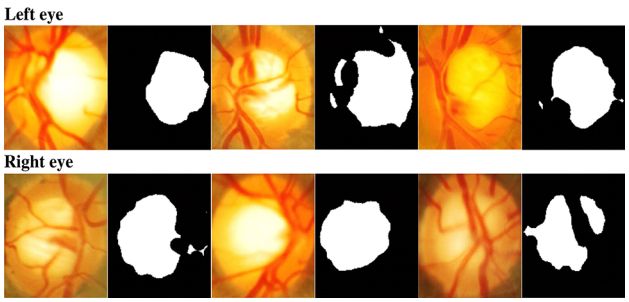

Fig. 5 Examples of the original and the thresholding results of the left or right eye

the setting of disc area is applied based on the result of the previous process.

Furthermore, we implement the disc segmentation. Firstly, we apply median filtering by the kernel size 3×3 based on red colour channel to decrease the influence of the blood vessels. Then, we apply Otsu's thresholding to segment the disc. To overcome the irregularity of the resulting disc, we perform opening by the strel size 30 followed by dilation by the strel size 5 to produce the appropriate disc size. Lastly, an ellipse fitting method is applied as in [6,16,30] to produce the boundary.

2.2 Cup segmentation

Initially, the disc area fitting is applied. The input is the information of disc boundary. It is used as a reference to form the ROI cup image (Fig. 3a). Subsequently, we perform a BVR process by closing operation in green colour channel with strel size 20 (Fig. 3b) to overcome the misclassification of the cup area caused by the existence of blood vessels, followed by conversion to greyscale image. To obtain the cup area, we propose structuring of the cup using Sobel method and cup masking by thresholding on greyscale image. The result is as shown in Fig. 3c, in which the structure of the cup visibly clearer, but still contains some noise. In this phase, the benefit of the BVR process is easily observed; an example of the cup structuring result with or without the BVR process is depicted in Fig. 4.

In order to remove noise and predict the cup area, we apply cup masking process. Firstly, we apply Otsu's thresholding (Fig. 3d). If the result is coincident with the obtained edge, then we repeat the thresholding process by increasing the threshold value until no area is coincident with the edge (Fig. 3e). Subsequently, we apply a translation process to shift the object in Fig. 3e to the centre of the image, assuming that the cup area is in the centre of the image. Furthermore, dilation operation is applied using strel with size 25 (Fig. 3f). The final step is setting the cup area, which is performed by AND-ing Fig. 3c, f, obtaining Fig. 3g. The set of pixels in Fig. 3g is used as the reference to obtain the boundary of the cup (Fig. 3h).

2.3 Eye detection

The input of this method is Fig. 3e and consists of several steps. First, we partition the thresholding result into two parts: left and right based on the central point of the image. Second, we compute the number of white pixels on both parts, then the last, we check the number of white pixels. If the number of white pixels on the left side is more than on the right side, then the image is the right eye and vice versa. Several examples of the result of this method are shown in Fig. 5.

Subsequently, we obtain the ISNT by measuring the distance between the boundary of the disc and the cup in the direction as shown in Fig. 1b. The ISNT are arranged as follows: I is at the bottom side, S is at the top side, while N and T are in the left or right side, respectively, depending on the eye. On right eyes, N is on the right side, while on left eyes it is on the left.

3 Methodology

3.1 Datasets

We use two datasets, namely D-I and D-II. D-I consists of 60 images by Nikon N150 digital camera incorporated by Carl Zeiss AG fundus camera with 30° field of view (FOV) and of dimension 2240 × 1488 pixels. D-II consists of 38 images by Nikon D90 digital camera incorporated by Topcon TRC-NW8 fundus camera with 45° FOV and of dimension 4288 × 2848 pixels. D-I and D-II were collected from Dr. YAP Eye Hospital and Dr. Sardjito Hospital in Yogyakarta, respectively. For all fundus images, the ground truth of CDR is obtained by three ophthalmologists, referred to Expert-1, Expert-2, and Expert-3 with experience of 2, 7, and 20 years, respectively, while the ground truths of boundaries of the disc and the cup are provided by Expert-2.

3.2 Experimental setup

We have conducted several types of the experiments. We compare the segmentation result of the disc and the cup produced by our method and Expert-2. Furthermore, we compare several parameters derived from the result of the segmentation of the disc and the cup, namely the v-CDR based on vertical diameters, the a-CDR based on area, and the *I–S–N–T* values. Lastly, we compare CDR values produced by our method (v-CDR) and by the three experts (CDR_{e_1}, CDR_{e_2}, CDR_{e_3}).

3.2.1 Disc–cup segmentation

The performance of our method is evaluated by comparing the area and the boundaries produced by the method and those by an expert, as has been done in a previous research [8].

Based on area the pixel-wise precision and recall values are used to evaluate the overlapping area between our method and the ground truth, and this is defined as follows:

$$\text{precision} = \frac{\text{TP}}{\text{TP} + \text{FP}}, \quad \text{recall} = \frac{\text{TP}}{\text{TP} + \text{FN}},$$

where TP (true positive) is the number of pixels segmented by the expert as disc/cup and classified as disc/cup by the method; FP (false positive) is the number of pixels segmented by the expert not as disc/cup but classified as disc/cup by the method; and FN (false negative) is the number of pixels segmented by the expert as disc/cup but classified not as disc/cup by the method. We also compute F_{score} as the harmonic mean of precision and recall. It lies between 0 and 1, and should have a high value for an accurate method. F_{score} is defined as folows:

$$F_{\text{score}} = \frac{\text{precision} \times \text{recall}}{\text{precision} + \text{recall}}.$$

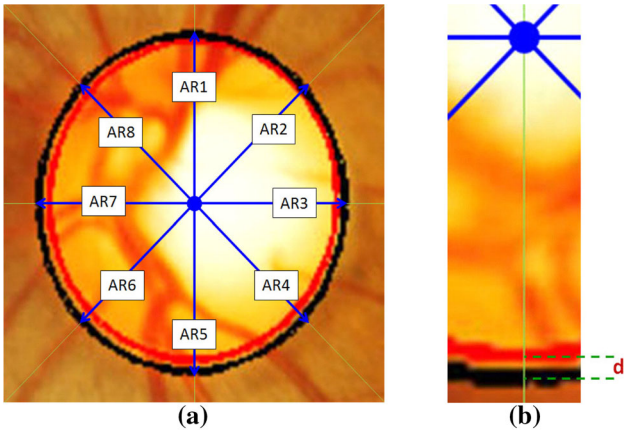

Fig. 6 **a** The reference point and the eight directions of measurement, **b** the detail of the distance between the two curves [C_{e} (*red*) and C_{m} (*black*)] (colour figure online)

Based on boundary the average boundary distance (μ_{d}) is used to evaluate the distance between the boundary produced by our method and by Expert-2 to examine the accuracy of the boundary localization result of our method. Here, we propose the measurement of μ_{d}, which is defined by (in pixels):

$$\mu_{\text{d}} = \frac{1}{r} \sum_{i=1}^{r} \left(|d_{\text{i}}^{e} - d_{\text{i}}^{m}| \right),$$

where d_{i}^{e} and d_{i}^{m} are the distance from the expert's curve centroid to the points on the expert's boundary (C_{e}) and our method's boundary (C_{m}), respectively, in the i-th direction. Similar to [31], μ_{d} is calculated based on the distance measurement in eight ($r = 8$) directions: 0°, 45°, 90°, 135°, 180°, 225°, 270°, and 315°, respectively. An overview of the reference point (the expert's curve centroid) and the eight directions (AR1–AR8) is shown in Fig. 6a. A more detailed view of the distance between C_{e} and C_{m} is shown in Fig. 6b.

3.2.2 Three derived parameters

Given n images, we compute the estimation error (means μ and standard deviation σ) of the difference (d) between the parameter obtained by Expert-2 (p_{e}) and the method (p_{m}) (v-CDR, a-CDR and *I–S–N–T*) to evaluate our method. The μ and σ are defined as:

$$d = |p_e - p_m|,\ \mu = \frac{\sum_{i=1}^{n} d_i}{n},\ \sigma = \frac{\sum_{i=1}^{n} \sqrt{(d_i - \mu)^2}}{n-1}.$$

3.2.3 v-CDR and CDR$_e$

The values of ground truth CDR (CDR$_e$) obtained by Expert-1, Expert-2, and Expert-3 based on the result of their visual estimations are compared to v-CDR. The performance of our method is expressed by the mean (μ_{err}) and standard deviations (σ_{err}). The evaluation method is defined as follows:

1. Calculate the average of CDR$_e$ (μ_{expert}) provided by each expert (x_i), with n is the number of experts:

$$\mu_{expert} = \frac{1}{n}\sum_{i=1}^{n} x_i.$$

2. Calculate the difference (d) between the CDR$_m$ and the μ_{expert}:

$$d = |\mu_{expert} - CDR_m|.$$

3. Perform step 1–2 for all images. Denote the difference d of image i as d_i.
4. The estimation error of the proposed method is defined as follows, with m is the number of images:

$$\mu_{err} = \frac{1}{m}\sum_{i=1}^{m} d_i,\ \sigma_{err} = \frac{1}{m-1}\sum_{i=1}^{m} \sqrt{(d_i - \mu_{err})^2}.$$

4 Experimental results

4.1 Disc segmentation

The illustration of several disc segmentation results depicted in Fig. 7. Those are obtained by Expert-2, our method and also two basic methods commonly used in previous researches: active contour and FCM. The red contour shows the segmentation result obtained by the expert, while the black one by the method. Column (a) depicts the original images and the remaining columns illustrate the segmentation result by the methods: (b) active contour, (c) FCM, and (d) our method, respectively. The first row depicts an example where all of the methods have been successfully segmented the disc due to the clear edge of the disc. This is indicated by the high value of F_{score} and the low value of μ_d. The second and third rows show that over-segmentation occurred to all methods, but our method is better than the others. They occurred because the presence of PPA is outside the disc.

The performance of all methods is summarized in Table 1. Based on this table, our method achieves the highest F_{score} of 0.96 for D-I, while for D-II FCM and ours achieve similar F_{score} of 0.96. However, our method is more robust than FCM since the average μ_d of our method is lower than FCM. Overall, our method achieves the highest of average F_{score} and the lowest of average μ_d for D-I, namely 0.96 and 7.7, and for D-II, namely 0.96 and 9.1. This shows that our method is more robust for D-I, because although both of them produce similar F_{score}, D-I produces lower value of μ_d than D-II.

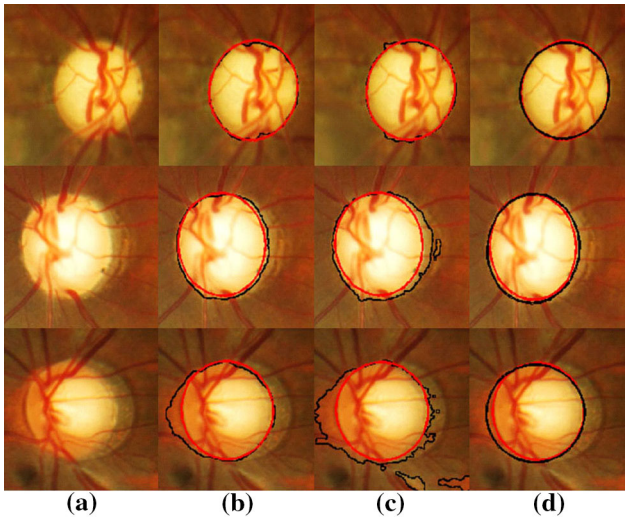

Fig. 7 Disc segmentation results: **a** original images, **b** active contour results, **c** FCM results, **d** our method result. *Red colour* boundary is obtained by the expert and *black colour* boundary is obtained by the method (colour figure online)

Table 1 The performance of disc segmentation (A) average F_{score}, and (B) average μ_d (in pixels)

	(A) F_{score}			(B) μ_d		
	D-I	D-II	Avg.	D-I	D-II	Avg.
Active contour	0.92	0.94	0.93	14.7	12.5	13.6
FCM	0.92	0.96	0.94	15.3	9.1	12.2
Our method	0.96	0.96	0.96	7.7	9.1	8.4

In the following, we compare our method to several methods reviewed in [32] as summarized in Table 2. The result of our method with respect to overlapping score is appreciable and comparable, although our method is lower than [8]. In terms of the average boundary distance (μ_d), however, our method is better than [8]. For our method μ_d is 8.4, while for [8] it is 11.1.

4.2 Cup segmentation

Several results of the cup segmentation obtained by Expert-2, thresholding, ellipse fitting and our method are shown in Fig. 8. Based on Fig. 8, we observe that the difficulty in cup

Table 2 Performance comparison of disc segmentation of other methods with our method

Methods	Datasets	Overlap ratio
Morphological, edge detection and features extraction [22]	DRIVE	0.76
Active contour [9]	DRIVE	0.76
Fuzzy convergence and Hough transform [33]	VARIA	0.93
Region-based active contour [8]	Local dataset	0.97
FCM [15]	Local dataset	0.93
Our method	Local dataset	0.96

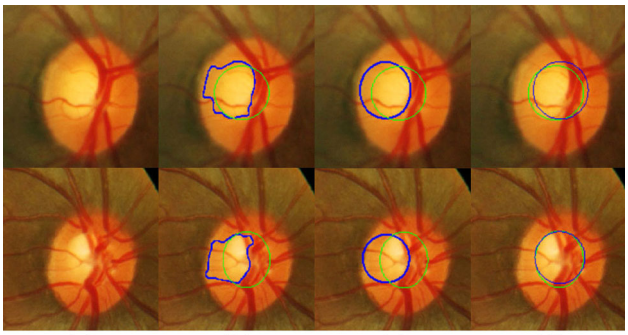

Fig. 8 Cup segmentation results: **a** original images, **b** threshold-based results, **c** ellipse fitting results, **d** our method result. *Green colour* boundary is obtained by the expert and *blue colour* boundary is obtained by the method (colour figure online)

Table 3 The performance of cup segmentation, (A) average F_{score}, and (B) average μ_{d} (in pixels)

	(A) F_{score}			(B) μ_{d}		
	D-I	D-II	Avg.	D-I	D-II	Avg.
Thresholding	0.72	0.65	0.68	27.5	38.3	32.9
Ellipse fitting	0.79	0.76	0.77	23.3	32.6	27.9
Our method	0.88	0.85	0.86	13.8	18.0	15.9

segmentation arises in determining the edge of the nasal and temporal sectors (both for left and right sides). In the nasal sector, misclassification of cup area is caused by the edge of cup becomes unclear because the main blood vessels cover the cup area. In the temporal sector, however, the edge of cup becomes unclear because the edge of the cup has smaller intensity difference than the edge of the disc. This occurs more frequently, and in turn, makes the cup's edge becomes unclear as shown in the second row.

The performance of all methods is reported in Table 3. It shows that our method is more superior than other methods based on the highest average F_{score} and the lowest average μ_{d}

Table 4 Performance comparison of cup segmentation of other methods with our method

Methods	Datasets	Overlap ratio
Model-based segmentation [21]	ORIGA	0.68
Superpixel classification [10]	SCES	0.76
Information of r-bends [8]	Local dataset	0.84
FCM [15]	Local dataset	0.89
Our method	Local dataset	0.86

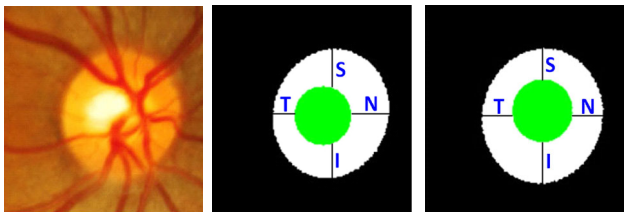

Original Image | v-CDR: 0.4490, a-CDR: 0.2233, ISNT: 93, 108, 113, 65 | v-CDR: 0.4569, a-CDR: 0.2323, ISNT: 119, 90, 90, 91

Fig. 9 An example of v-CDR, a-CDR and *I–S–N–T* parameters obtained by the single expert and our method on the left eye

achieved. The average F_{score} and μ_{d} for D-I are 0.88 and 13.8, respectively, while for D-II are 0.85 and 18.0, respectively. The value of F_{score} decreases, while the average boundaries increase. These indicate that cup segmentation is indeed more difficult than disc segmentation.

The summary of the comparison result between our method with other methods is shown in Table 4. The result of our method with respect to overlapping score is competitive. Although our method is lower than [15], we have used a much larger dataset, which consists of 98 images, compared to 27 in [15].

4.3 Three derived parameters

Parameters v-CDR, a-CDR, and *I–S–N–T* can be directly derived from the disc–cup segmentation results, which are useful for glaucoma evaluation. The v-CDR parameter reflects the accuracy of segmentation only in vertical direction, while the a-CDR parameter indicates the overall segmentation accuracy achieved in all directions. In order to improve the diagnosis of glaucoma based on the compatibility of ISNT rule, we also derive *I–S–N–T* parameters. An example of the parameters produced by the single expert compared to our method is shown in Fig. 9.

The performance of our method is expressed by the estimation error ($\mu \pm \sigma$) of v-CDR, a-CDR, and *I–S–N–T* values of all retinal fundus images in D-I and D-II. The evaluation results of v-CDR and a-CDR are shown in Table 5, while *I–S–N–T* is in Table 6.

Table 5 Estimation error of v-CDR and a-CDR

	v-CDR		a-CDR	
	μ	σ	μ	σ
D-I	0.04	0.04	0.06	0.05
D-II	0.04	0.04	0.06	0.04
Avg.	0.04	0.04	0.06	0.05

Table 6 Estimation error of *I*–*S*–*N*–*T* (in pixels)

	I		*S*		*N*		*T*	
	μ	σ	μ	σ	μ	σ	μ	σ
D-I	12.2	10.1	11.9	9.7	20.0	14.8	15.5	13.3
D-II	20.4	13.7	13.3	9.9	22.5	20.0	23.4	14.7
Avg.	16.3	11.9	12.6	9.8	21.2	17.4	19.4	14.0

Table 5 shows that the estimation errors reflected by the average mean (μ) and the standard deviation σ of v-CDR is smaller than that of a-CDR. Based on this, we can conclude that with respect to the glaucoma evaluation via v-CDR or a-CDR, our method is more accurate in obtaining v-CDR parameter. Moreover, experts use this parameter as the main indicator in evaluating glaucoma.

The estimation error of *I*–*S*–*N*–*T* parameter is summarized in Table 6. The table shows that the largest inaccuracies occur in the nasal (N) and temporal (T) sectors. This matches the previous conclusion with respect to cup segmentation that stated that the difficulty in cup segmentation arises in determining the edge of the nasal and temporal sectors. Figure 9 depicts an example fundus image, where v-CDR is 0.4490, which indicates that the eye is healthy. However, the eye does not follow the ISNT rule (namely, $I = 93$, $S = 108$, $N = 113$, and $T = 65$). Based on this, the image is diagnosed as glaucoma and it proves that v-CDR alone cannot be used to conclusively evaluate glaucoma. This shows that the increasing precision of measurement result in the values of CDR and ISNT certainly impacts the accuracy of glaucoma diagnosis result. Furthermore, a high precision result may allow us not just to detect the existence of glaucoma in a given image, but also to classify the glaucoma based in its severity (stages).

4.4 v-CDR and CDR_e

The CDR values of each retinal fundus image collected from the three experts may differ among themselves. Figure 10 shows three examples of the variation of the CDR_e obtained by three experts and the v-CDR. The performance of our method is indicated by the estimation error ($\mu_{err} \pm \sigma_{err}$). The estimation error should have a low value close to 0. A lower value not only indicates that the subjectivity of diagnosis from the three experts is smaller, but also indicates

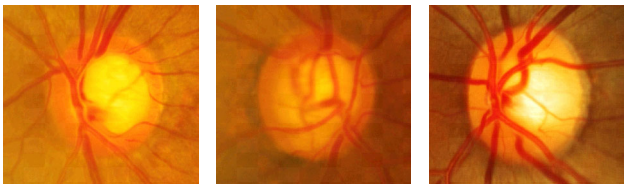

Fig. 10 The CDR_e and the CDR_m of several fundus images

that the performance of the segmentation method is better. Our method obtains the lowest values for D-I and D-II at 0.04 ± 0.03 and 0.04 ± 0.04, respectively. This indicates that the value of v-CDR is closer to 0 and falls within the disputed region, namely the region where the three experts disagree. The disagreement in estimating the edge of the cup in the inferior and/or the superior sectors causes the variation of the CDR_e obtained by three experts. The first image has no variation of the CDR_e since it has the clearest edge of the cup area when compared to the second and third images as shown in Fig. 10.

5 Conclusion

In this research, a disc localization method has been proposed for a computer-assisted glaucoma evaluation. Thresholding with a high threshold value is implemented based on green channel of RGB image, which is then used as a reference to predict the initial disc area. Subsequently, a border masking is performed by thresholding based on red colour space followed by edge detection. These all are to avoid misclassifying areas. Incorporating these processes results in a robust disc localization process. This localization process, in turn, supports the performance of the disc segmentation. We also propose a robust method for cup segmentation by forming the structure of cup based on edge detection and cup masking based on thresholding of green channel.

This research is different to previous approaches, which mostly focus on estimating the CDR value to determine whether a given eye is normal or suffers glaucoma. Our method, on the other hand, estimates not only the CDR value, but also the ISNT values; and this improves the overall accuracy. Overall, the obtained result of our method based on the three derived parameters is a clear evidence of a promising novel method for glaucoma evaluation. For future work, there are other features that can be extracted in fundus images such as PPA or RNFL since CDR alone cannot be used to conclusively evaluate glaucoma.

Acknowledgements The authors would like to thank Dr. Sardjito Hospital and Dr. YAP Eye Hospital in Yogyakarta, Indonesia, for providing the fundus images.

References

1. Quigley, H.A.: Number of people with glaucoma worldwide. Br. J. Ophthalmol. **80**(5), 389–393 (1996)
2. Choplin, N.T., Lundy, D.C. (eds.): Atlas of Glaucoma, 2nd edn. Informa Healthcare, London (2007)
3. Hatanaka, Y., Fukuta, K., Muramatsu, C., Sawada, A., Hara, T., Yamamoto, T., Fujita, H.: Automated measurement of cup-to-disc ratio for diagnosing glaucoma in retinal fundus images. IFMBE Proc. 25/XI **25**, 198–200 (2009)
4. Muramatsu, C., Nakagawa, T., Sawada, A., Hatanaka, Y., Hara, T., Yamamoto, T., Fujita, H.: Determination of cup and disc ratio of optical nerve head for diagnosis of glaucoma on stereo retinal fundus image pairs. Proc. SPIE **7260**, 1–8 (2009)
5. Mary, M.C.V.S., Rajsingh, E.B., Jacob, J.K.K., Anandhi, D., Amato, U., Selvan, S.E.: An empirical study on optic disc segmentation using an active contour model. Biomed. Signal Process. Control **18**, 19–29 (2015)
6. Mittapalli, P.S., Kande, G.B.: Segmentation of optic disk and optic cup from digital fundus images for the assessment of glaucoma. Biomed. Signal Process. Control **24**, 34–46 (2016)
7. Fondón, I., Núñez, F., Tirado, M., Jiménez, S.: Automatic cup-to-disc ratio estimation using active contours and color clustering in fundus images for glaucoma diagnosis. In: International Conference on Image Analysis and Recognition, pp. 390–399. Springer (2012)
8. Joshi, G.D., Sivaswamy, J., Krishnadas, S.R.: Optic disk and cup segmentation from monocular color retinal images for glaucoma assessment. IEEE Trans. Med. Imaging **30**(6), 1192–1205 (2011)
9. Tjandrasa, H., Wijayanti, A., Suciati, N.: Optic nerve head segmentation using hough transform and active contours. Telkomnika **10**(3), 531–536 (2012)
10. Cheng, J., Liu, J., Xu, Y., Yin, F., Wing, D., Wong, K., Tan, N.M., Tao, D.: Superpixel classification based optic disc and optic cup segmentation for glaucoma screening. IEEE Trans. Med. Imaging **36**(6), 1019–1032 (2013)
11. Dutta, M.K., Mourya, A.K., Singh, A., Parthasarathi, M., Burget, R., Riha, K.: Glaucoma detection by segmenting the super pixels from fundus colour retinal images. In: 2014 International Conference on Medical Imaging, m-Health and Emerging Communication Systems (MedCom), pp. 86–90. IEEE (2014)
12. Tan, N.M., Xu, Y., Goh, W.B., Liu, J.: Robust multi-scale superpixel classification for optic cup localization. Comput. Med. Imaging Graph. **40**, 182–193 (2015)
13. Ho, C.Y., Pai, T.W., Chang, H.T., Chen, H.Y.: An automatic fundus image analysis system for clinical diagnosis of glaucoma. In: Intelligent, and Software Intensive Systems an International Conference on Complex (2011)
14. Kavitha, S., Karthikeyan, S., Duraiswamy, K.: Early detection of glaucoma in retinal images using cup to disc ratio. In: 2010 2nd International Conference on Computing, Communication and Networking Technologies, vol. 2, pp. 1–5. IEEE (2010)
15. Khalid, N.E.A., Noor, N.M., Ariff, N.: Fuzzy c-means (FCM) for optic cup and disc segmentation with morphological operation. Proc. Comput. Sci. **42**, 255–262 (2014)
16. Narasimhan, K., Vijayarekha, K.: An efficient automated system for glaucoma detection using fundus image. J. Theor. Appl. Inf. Technol. **33**(1), 104–110 (2011)
17. Nayak, J., Acharya, U.R., Bhat, P.S., Shetty, N., Lim, T.C.: Automated diagnosis of glaucoma using digital fundus images. J. Med. Syst. **33**, 337–346 (2008)
18. Lu, S.: Accurate and efficient optic disc detection and segmentation by a circular transformation. IEEE Trans. Med. Imaging **30**(12), 2126–2133 (2011)
19. Sinha, N., Babu, R.V.: Optic disk localization using L1 minimization. In: Proceedings of the 19th IEEE International Conference on Image Processing (ICIP 12), pp. 2829–2832 (2012)
20. Welfer, D., Scharcanski, J., Kitamura, C.M., Pizzol, M.M.D., Ludwig, L.W.B., Marinho, D.R.: Segmentation of the optic disk in color eye fundus images using an adaptive morphological approach. Comput. Biol. Med. **40**(2), 124–137 (2010)
21. Yin, F., Liu, J., Wing, D., Wong, K., Tan, N.M., Cheung, C.: Automated segmentation of optic disc and optic cup in fundus images for glaucoma diagnosis. In: 2012 25th International Symposium on Computer-Based Medical Systems (CBMS) (2012)
22. Aquino, A., Gegundez-Arias, M.E., Marn, D.: Detecting the optic disc boundary in digital fundus images using morphological, edge detection, and feature extraction techniques. IEEE Trans. Med. Imaging **29**(11), 1860–1869 (2010)
23. Pourreza-Shahri, R., Tavakoli, M., Kehtarnavaz, N.: Computationally efficient optic nerve head detection in retinal fundus images. Biomed. Signal Process. Control **11**, 63–73 (2014)
24. Sinthanayothin, C., Boyce, J.F., Cook, H.L., Williamson, T.H.: Automated localisation of the optic disc, fovea, and retinal blood vessels from digital colour fundus images. Br. J. Ophthalmol. **83**, 902–910 (1999)
25. Ahmad, H., Yamin, A., Shakeel, A., Gillani, S.O., Ansari, U.: Detection of glaucoma using retinal fundus images. In: 2014 International Conference on Robotics and Emerging Allied Technologies in Engineering, iCREATE 2014—Proceedings, pp. 321–324 (2014)
26. Marin, D., Gegundez-Arias, M.E., Suero, A., Bravo, J.M.: Obtaining optic disc center and pixel region by automatic thresholding methods on morphologically processed fundus images. Comput. Methods Programs Biomed. **118**(2), 173–185 (2015)
27. Foracchia, M., Grisan, E., Ruggeri, A.: Detection of optic disc in retinal images by means of a geometrical model of vessel structure. IEEE Trans. Med. Imaging **23**(10), 1189–1195 (2004)
28. Rahman, R., Kabir, S.M.R, Quadir, A.: Intelligent detection of foveal zone from colored fundus images of human retina through a robust combination of fuzzy-logic and active contour model. In: Awad, A.I., Hassaballah, M. (eds.) Image Feature Detectors and Descriptors, pp. 305–344. Springer, Cham (2016)
29. Ahmed, M.I., Amin, M.A.: High speed detection of optical disc in retinal fundus image. SIViP **9**, 77–85 (2015)
30. Jayanthi, G., Sagayee, G.M.A., Arumugam, S.: Glaucoma detection in retinal image using medial axis detection and level set method. Int. J. Comput. Appl. **93**(3), 42–48 (2014)
31. Fumero, F., Alayon, S., Sanchez, J.L., Sigut, J., Gonzalez-Hernandez, M.: RIM-ONE: an open retinal image database for optic nerve evaluation. In: Proceedings—IEEE Symposium on Computer-Based Medical Systems, pp. 2–7 (2011)
32. Almazroa, A., Burman, R., Raahemifar, K., Lakshminarayanan, V.: Optic disc and optic cup segmentation methodologies for glaucoma image detection: a survey. J. Ophthalmol. **2015**, 1–28 (2015)
33. Fraga, A., Barreira, N., Ortega, M., Penedo, M.G., Carreira, M.J.: Precise segmentation of the optic disc in retinal fundus images. In: Moreno-Díaz, R., Pichler, F., Quesada-Arencibia, A. (eds.) Computer Aided Systems Theory – EUROCAST 2011. EUROCAST 2011. Lecture Notes in Computer Science, vol 6927. Springer, Berlin (2012)